Materials Research Express

Multilayered ZnO/TiO_2 nanostructures as efficient corrosion protection for stainless steel 304

To cite this article before publication: Said Boukerche *et al* 2019 *Mater. Res. Express* in press https://doi.org/10.1088/2053-1591/ab042f

Multilayered ZnO/TiO_2 Nanostructures as Efficient Corrosion Protection for Stainless Steel 304

S. Boukerche[1], A. Himour[1], M.Bououdina[2,*], F. Bensouici[3] and S. Ouchenane[1]

[1]Laboratoire d'Ingénierie des Surfaces (LIS) – University Badji Mokhtar - Annaba, Algeria

[2]Department of Physics, College of Science, University of Bahrain, Kingdom of Bahrain

[3]Department of Physics, URMPE, University M'Hamed Bougara of Boumerdes, Algeria

* Corresponding author: mboudina@gmail.com (M. Bououdina, PhD)

Abstract

ZnO/TiO_2 coatings are deposited onto 304 stainless steel substrates by using sol-gel dip-coating technique followed by subsequent annealing. X-ray diffraction analysis reveals nanocrystalline ZnO and TiO_2 phases for all multilayered films except $1ZnO/1TiO_2$ with amorphous nature. Optical microscopy images show the presence of some streaks, holes, scratches and micro-traces, meanwhile the obtained coatings present different colours, from grey to yellowish. Scanning electron microscopy observations indicate that the deposited films are smooth, uniform, with low level of cracks. Surface topography analysed by atomic force microscopy confirms the smoothness of the coatings; the roughness is very low 0.764 – 5.166 nm. UV-vis spectroscopy analysis indicates that the energy bandgap varies according the nature and order of the deposited layers; 3.32 eV for $1TiO_2/1ZnO$ up to 3.68 eV for $2TiO_2/2ZnO$. Corrosion tests were carried out, especially potentiostatic (EIS) and potentiodynamic (Tafel plots). The corrosion protection performance for stainless steel 304 (304SS) has been evaluated in 3% wt NaCl solution. The obtained results reveal that the $1TiO_2/1ZnO$ multilayered thin film exhibits a remarkable improvement in anticorrosion performance; reaching a very high efficiency protection of 98 %. This has been attributed to the double protective layer (TiO_2-Tetragonal/ZnO-Hexagonal) preventing the diffusion of corrosive ions through the surface.

Keywords: Stainless Steel; ZnO; TiO_2; Coating; Corrosion; Electrochemical impedance spectroscopy.

1. Introduction

Stainless steel 304 (SS 304) is widely used in various industries and applications, due to its excellent corrosion resistance, good mechanical properties, and relatively low cost. It resists against corrosion in a variety of aggressive environments. Nevertheless, this Fe-based material, once attacked by corrosion, causes more damages and the inevitably problem is that corrosion cannot be totally eliminated. But its effect can be reduced with the use of different methods such as inhibitors [1], protective films and organic/inorganic coatings deposited onto the metal surface.

Nowadays, nanoparticles coatings are extensively used to protect metals against corrosion. For this purpose, numerous oxides such as ZnO, TiO_2, ZrO_2, Al_2O_3, SiO_2, etc. have been proposed in order to improve the surface properties of metals [2-7]. Meanwhile, several techniques are used for the deposition of coating layer onto the surface of stainless steel, like physical vapour deposition (PVD) [8], chemical vapour deposition (CVD) [9], electrochemical deposition [10] and sol–gel process [11]. During the last decades, sol-gel method is widely used for the deposition of nanomaterials [12,13]. It can be combined with spray, spin-coating and dip-coating processes for the preparation of thin films. Sol-gel dip-coating is known as environmentally friendly technique and offers several advantages, such as simplicity, low-cost, cover large area of substrate, better control of shape and size, effective doping, etc. [13].

In the literature, several researches were devoted to the depositions of anti-corrosion coating layers onto metals and alloys. In particular, the use of metal oxide semiconductors as protective coatings is gaining great interest because of their interesting properties in addition to the low cost as well as facile deposition of large surface areas. The deposition of TiO_2 [14-16] and ZnO [17-19] onto SS 304 has been

rarely investigated. The effect of number of layers (1 and 3) of TiO_2 prepared with and without PEG was studied. The obtained results indicated the presence of both anatase and rutile phases, with the formation of uniform/compact coating without cracks while roughness increases from 2.10nm for 1 layer up to 5.41nm for 3 layers. The electrochemical tests showed an improvement of protective properties with the increase of the film thickness (number of layers) [9].WO_3 and TiO_2 nanoflakes were studied by electrodeposition method. Monoclinic WO_3 crystalline and anatase TiO_2 phase appeared for annealed WO_3 and TiO_2 composite film at 450°C in addition to WO_3. FESEM observations indicate the apparition of WO_3 nanoflake-arrays with thickness about 30 nm. Electrochemical tests proved an ability to prevent 316SS from pitting corrosion [15]. Another study investigated the performance of TiO_2 thin film as a photoanode and evaluated the addition of sulphur on the corrosion of SS 304. XRD analysis indicated the presence of anatase and rutile phases, meanwhile SEM revealed the presence of cracks and microsize porosity. A high corrosion performance of S-doped TiO_2 in comparison with pure TiO_2 was obtained [16].

On the other side, the progress of particles size of the composite ZnO/GPTMS (0.1, 0.5, 1% (w/w)) nanoparticles on the corrosion protection of tinplate with tin coating (as a substrate), was investigated [17]. SEM micrographs revealed a homogeneous distribution of particles where as a damaged surface for the undoped film and a corroded area for doped film where zinc nanoparticles were accumulated around the cracks. Impedance measurements indicated that ZnO addition improve the thin film behaviour against corrosion protection [18]. XPS showed the presence of both species Sn^{2+}/Sn^{4+}. Moreover, the photocathodic characteristics of ZnO coating deposited by spray pyrolysis technique at (200 and 400°C) and its corrosion protection were studied

[19]. SEM images showed a dense nanopowder coating at 200°C and loosely-compacted nano-granular needle-like structures at 400°C. Electrochemical tests (open circuitpotential, OCP) revealed that ZnO coating could not provide a cathodic protection to SS304 in dark and UV conditions. Finally, a polymeric(poly(dimethylsiloxane) - PDMS)/ZnO nanocomposite prepared by spin coating has been investigated as corrosion protection of Q235 steel [20]. It was found that the roughness of PDMS/ZnO increases drastically with the amount of perfluorodecyltrichlorosilane (FDTS) [21]; i.e. 15 to 99 nm for 0.0 to 0.40 g, respectively. Meanwhile, the hydrophobic character of the coatings was confirmed by water contact measurements. Electrochemical tests showed that 0.10 FDTS had the highest barrier performance and lowest rate of degradation. Bode plots indicated three different degradation times while Nyquist plots showed the appearance of a new time constant [20].

In this paper, four layers of alternating ZnO/TiO_2, layer by layer and two layers by two layers were deposited onto 304 SS substrates by using sol-gel spin coating procedure. The reasons for using alternating layers of ZnO/TiO_2 are: (i) to have a double corrosion protection performance when forming a layered structure, as ZnO and TiO_2 possess different corrosion characteristics; (ii) ZnO (Hexagonal) and TiO_2 (Tetragonal) possess different crystal structures, thereby when superposed over each other, it is expected that a "high compaction rate" can be achieved with effective atomic arrangement barrier inhibiting the diffusion of corrosive ions present in the medium (in this case Cl^-) within the substrate; and more importantly (iii) no previous research work reported the use of multilayered approach in order to improve the corrosion resistance, usually ZnO and TiO_2 are used separately, which is the novelty of this research work.

The effect of the nature of coating layer on the anti-corrosion performance was investigated in terms of potentiostatic and potentiodynamic tests. The obtained results are discussed in terms of crystal structure as well as surface morphology and topography of the coatings, and the thin films behaviour against corrosion protection.

2. Experimental Part

2.1. Preparation of Stainless Steel Surface

Parallelepiped shaped (10 × 20 × 1) mm 304 Stainless Steel (SS 304) substrates were used. Prior to deposition, the substrates were mechanically polished successively with abrasive papers of different grit 600, 800, 1000, 1200, 2000 and 2400. The substrates were then ultrasonically cleaned with acetone and deionized water respectively for 10 min at 60°C and, finally, dried at 100°C for 1 h before deposition process.

2.2. Preparation of ZnO and TiO_2 Solutions and Film Deposition

The ZnO solution was prepared using zinc acetate dihydrate ($Zn(CH_3COO)_2.2H_2O$) as precursor (Fluka, >99.0%), ethanol and monoethanolamine (C_2H_7NO, MEA. For preparing TiO_2 sol, titanium (IV) n-propoxide ($Ti(OCH_2CH_2CH_3)_4$)-NPT (Alfa Aesar GmbH & Co KG, 98+%) was dissolved in a solution containing ethanol, water and nitric acid (69% Sigma Aldrich). In the solutions, Zn^{2+} concentration was chosen as 0.4 M [22] and Ti^{4+} concentration as 0.7M [23]. The solutions was successively stirred for 1 h and aged for 24 h. ZnO and TiO_2 nanoparticles coatings were deposited by dip-coating method. The substrates were immersed in the sol and then withdraw at a speed of 1 $mm{\cdot}s^{-1}$. The coated substrates were heated at 400°C for 10 min. The dip coating and drying processes were repeated four times to carry out the desired thickness. Finally, the obtained thin films were calcined at 450°C for 1 h. In this study, layer-by-layer (LbL) four films were deposited as follow: one layer of ZnO followed by one

layer of TiO_2 ($1ZnO/1TiO_2$) and alternately; two layers of ZnO followed by two layers of TiO_2 ($2ZnO/2TiO_2$) and alternately.

2.3. Characterisations of films

The structure and crystalline phase of the obtained coatings were checked with X-Ray diffraction (XRD) technique using Philips X'Pert diffractometer equipped with Cu-Kα radiation (λ=1,5418 Å). Morphological observations were performed by optical microscopy using Nikon ECLIPSE LV150N and scanning electron microscopy (SEM) using FEI QUANTA 250. Optical absorbance spectral were recorded by using Shimadzu UV-Vis 3600 plus spectrophotometer in UV–Vis–NIR spectral region (200–800) nm. Surface topography and roughness were examined using an Oxford Instrument atomic force microscope (AFM) Asylum Research MFP3D.

2.4. Electrochemical Testing

The electrochemical measurements were carried out using three electrode assembly, Potentiostat/Galvanostat, model PGSTAT302N controlled by a PC through the general purpose electrochemical system (GPES) software provided by AUTOLAB. The experiments were carried out using saturated calomel electrode (SCE) as reference electrode, platinum (Pt) plate as counter electrode and coated stainless steel substrates as working electrode. The experiments were performed using a scan rate of 1 mV/s commencing at a potential above 1000 mV more active than the stable open circuit potential.

All the measurements were carried out at room temperature (30± 1°C) in near neutral 3 wt.% NaCl (0.5 M) aqueous solution. Before starting the measurements, the specimen was left in the solution for 30 min to attain a steady state which was indicated by a constant potential.

Electrochemical impedance spectroscopy (EIS) measurements were conducting in 0.5 M NaCl after 1 h immersion at open circuit potential (OCP). All experiments were performed in the frequency range from 100 kHz to 10 mHz with an amplitude of the voltage perturbation equal to 10 mV rms.

Tafel plots were recorded in the potential range -1000 mV – 1000 mV with a scan rate of 1 mV/S.

The linear polarization resistance (LPR) measurements were carried out by recording the electrode potential ±10 mV around open circuit potential with 1 mV/s scan rate. The polarization resistance (Rp) was determined from the slope of the current–potential curves obtained.

3. Results and discussion

3.1 X-ray Diffraction Analysis

Fig.1 displays the evolution of XRD patterns of ZnO/TiO_2 multi-layers. One can notice the formation of amorphous (presence of "halo" in the small 2θ-range) and nanocrystalline (broad peaks with low intensity) phases.

For $1ZnO/1TiO_2$, only amorphous phase is formed. However, when changing the order of the deposited layers, for instance $1TiO_2/1ZnO$, the amorphous remains while one major broad peak with very low intensity emerges at 2θ= 34.375°. This peak represents the major (002) reflection of the hexagonal wurtzite-type structure of ZnO phase, in agreement with JCPDS card N° 73-8765.

Interesting, for $2ZnO/2TiO_2$, the amorphous remains while new broad peaks with low intensity emerges at 2θ= 25.425°. This peak was indexed as (101) reflection of TiO_2 phase with anatase structure, in agreement with JCPDS card N°. 21-1272. Finally, for $2TiO_2/2ZnO$, in addition to the amorphous phase, few broad peaks with variable

intensity appear at 2θ=25.225°, 34.425°, 38.025°, 47.925° and 62.975°. The above peaks have been indexed within wurtzite ZnO and anatase TiO_2 phases. It is noteworthy to highlight that both phases reveal preferred orientation along (002) plane for ZnO and (101) plane for TiO_2.

From the above results, the following remarks can be emphasized: (i) layer-by-layer (1LbL) does not favour the crystallization of both ZnO and TiO_2 phases; (ii) for 2layers-by-2layers (2Lb2L) , the crystallization is more favourable for ZnO phase; (iii) it seems that ZnO inhibit the crystallization of TiO_2 for the deposition LbL.

The crystallite size and microstrain have been calculated, based on the main reflections (101) for TiO_2 and (002) for ZnO by using the high score program. From Table 1, it can be noticed that: (i) 15 nm for 1LbL than increases drastically by more than 4 times reaching 68 nm for 2LbLfor TiO_2/ZnO. The crystallite size (CS) of TiO_2 is very smaller than that of ZnO; i.e. 9 nm; (ii) meanwhile, the microstrain (MS) of ZnO is reduced by 4 times; i.e. 0.86% to 0.19 % for 1LbL and 2LbL respectively and that of TiO_2 is very high compared to ZnO reaching 1.80%.For the system ZnO/TiO_2, 2LbL shows the lowest microstrain of 2.5%.

The above observations in terms of formation of amorphous/nanocrystalline phases as well as the evolution of the crystallite size and microstrain, can be attributed to several factors including: (i) the grain growth of ZnO crystallites along a preferred orientation (002) over TiO_2 (101) plane (CS_{ZnO}=15nm) seems energetically more favourable compared to the amorphous TiO_2 (CS_{ZnO}=68 nm); (ii) the development of microstrain along the multilayers will be affected by the mismatch between the lattice parameters of ZnO (a=b=3.251 Å and c=5.210Å [24]) and TiO_2 (a=b=3.805 Å and c=9.549Å [25]) in addition to the planes of preferred orientations.

Both crystallite size and microstrain depend on the nature and crystal structure of the compound in addition to the number of deposited layers; (i) 16 nm and 0.145% for 4 layers of TiO_2 [23] while (ii) 14 nm and 0.340% for 5 layers of ZnO [24].

3.2 Optical Microscopy Observations

The optical microscope images (Figure 2) show the surface of SS 304 substrate and coated with alternating layers of ZnO and TiO_2.It can be observed the presence of streaks, holes, scratches and micro-traces due to poor polishing although the adopted procedure. Interestingly, the images present different colours that allow identifying the nature of the appropriate coating. It can be seen that the coating has penetrated these holes, scratches and micro-tracks. The obtained coatings have specific colours caused by the 4 alternating thin layers of ZnO and TiO_2: (i) yellowness colour for $1ZnO/1TiO_2$ that becomes darker for $2ZnO/2TiO_2$ (ii) blue-grey colour for $1TiO_2/1ZnO$ that becomes darker for $2TiO_2/2ZnO$.

The appearance of such colours resulted from many factors including mainly: (i) topography (smoothness/roughness) of surface;(ii) morphology and size of grains; (iii) the interaction between the white light and the type of coating layer (ZnO and TiO_2); and (iv) the thickness of the coatings. Physically, the colour of the coating is due to the absorption of the white light by the thin film. This can be explained by the fact that each coating acquires a specific refractive index.

3.3 Morphological Observations by SEM

The morphology of the surface of stainless steel SS304 substrate and multilayer coatings (ZnO/TiO_2) was investigated by SEM. The micrographs shown in Figure 3 indicate that the bare stainless steel SS 304 substrate presents uniform surface with low

level of streaks and holes, while after coating, the thin deposited films are smooth, uniform, without cracks as previously mentioned in optical microscopy observations (Figure 2). The observed microstructural defects are more beneficial for the adherence of the deposited coatings onto the substrate SS 304.

For a further insight into surface analysis, higher magnifications images reveal the apparition of holes and streaks covering the entire films, which explain the penetration of the prepared mixture into the holes and streaks. Also, one can distinguishes that the composite multilayered films demonstrate the same morphology

3.4 Surface Topography Analysis by AFM

In order to characterize the surface morphology at high resolution, the specimens were subject to AFM measurements. The AFM images are obtained in tapping mode by oscillating the tip over the surface at its resonance frequency. This method is employed in order to cancel the friction forces between the tip and the samples preserving the tip apex (sharp tip). All topography of samples is presented in Figure 4. It can be observed that the surface of the steel substrate presents a smooth surface with very fine scratches; which indicated a good mechanical polishing of the surface of the substrate. The ZnO/TiO_2 and $2ZnO/2TiO_2$ shown a high density of nanosized peaks (or bumps) forming an ordered network. In the case of TiO_2/ZnO and $2TiO_2/2ZnO$ samples, the results show that thin films exhibit waviness surface texture and the surface of the film presents also peaks but are randomly distributed formed lines of nano-peaks and has the shape of the hills and valleys.

Also, the Atomic force microscopic analysis is ideal for quantitatively measuring the nanometric dimensional surface roughness and deducts the film surface properties using parameters such, root mean square roughness (RMS), surface skewness and

surface kurtosis. These are parameters that allow insight into the surface properties and quality and the data are reported in Table 2. All surfaces are smooth with an RMS below 5 nm, which should enhance their optical transparency (see optical measurements). It is observed that ZnO/TiO_2 thin films are very smooth than TiO_2/ZnO.

The surface skewness of the films is positive which confirms the presence of numerous bumps except the TiO_2/ZnO samples show a negative skewness indicated that the surface is more planar and valleys are predominant. Moreover, the surface kurtosis corresponds to a measure of surface sharpness, the kurtosis of the TiO_2/ZnO and $2TiO_2/2ZnO$ films (2.77 and 1.22 nm respectively) is very high compared to that of the ZnO/TiO_2 and $2ZnO/2TiO_2$ films (0.65 and 0.13 nm respectively), which confirms the peakedness of its surface.

3.5 Optical Properties

The spectral optical transmittance T(λ) and reflectance R(λ) were examined at normal incidence in UV-VIS-NIR spectral region (200–850 nm) and measured with a Shimadzu UV- vis 3600 spectrophotometer and showed in Figure 5 (a and b). The spectra reveal very pronounced interference effects in the transparency region 380–850 nm with sharp fall of transmittance at the band edge. The appearance of interferences reveals the good homogeneity of the obtained coatings [26]. At room temperature, optical absorption spectra of SS 304 coated with ZnO/TiO_2 thin films have been calculated by using eq. 1 (Figure 5c) in order to determine the absorption coefficient and optical energy gap (Eg). Knowing the film thickness (t), the optical absorption coefficient (α) could be determined from the measurements of T(λ) and R(λ) by using eqs. (2, 3 and 4) [27,28]:

$$A = ln\frac{(1-R^2)}{T} \ldots\ldots\ldots\ldots\ldots\ldots\ldots\ldots (1)$$

$$T \cong (1-R^2)e^{-\alpha t} \ldots\ldots\ldots\ldots\ldots\ldots\ldots\ldots (2)$$

$$\ln(T) \cong ln(1-R^2) - \alpha t \ldots\ldots\ldots\ldots\ldots (3)$$

$$\alpha = \frac{1}{t} ln\frac{(1-R^2)}{T} \ldots\ldots\ldots\ldots\ldots\ldots\ldots\ldots (4)$$

In order to determine the optical absorption coefficient (α), some references in the literature use the following formula with neglecting the reflectance effect [25]:

$$\alpha(\lambda) = \frac{A(\lambda)}{t} = \frac{1}{t} ln\left(\frac{1}{T}\right) \ldots\ldots\ldots\ldots\ldots\ldots\ldots\ldots (5)$$

Figure 5c shows the dependence of absorption spectra upon the wavelength of SS 304 coated with ZnO/TiO_2 alternating thin films. This figure reveals the presence of an absorption edge in the ultra-violet (UV) region. The position of the absorption edge depends on the type of thin films; it is situated between 325 to 340 nm. Furthermore, the optical absorption coefficient (α) has high values for all the studied multilayered coatings (in the range10^5-10^6 nm^{-1}).

The optical direct and indirect bandgap Eg is evaluated according to the well-known Tauc relation [29]:

$$\alpha E = A_{Op}(E - E_g)^n \qquad (6)$$

where A_{Op} is constant of the film. The exponent n is equal to 2 and1/2 for indirect and direct band gap, respectively. Thus, according to Tauc method, the plot of $(\alpha.E)^{0.5}$vs$h\nu$ as shown in Figure 6a gives the value of indirect bandgap, while the plot of $(\alpha E)^2$vs$h\nu$ as shown in Figure 6b gives the value of direct bandgap.

The appearance of interference fringes result from reflections on the levels of film/substrate and film/air interfaces. This indicates that the obtained films are sufficiently thick.

The values of energy bandgap vary according the type of the coating. It can be noted that for ZnO/TiO_2 thin film layer by layer and alternately are 3.57 and 3.32 eV; and for ZnO/TiO_2 thin film 2layer by 2layer and alternately are 3.44 and 3.68 eV. This variation is attributed to the disappearance of the impurities and defects. When the energy bandgap increases, the defects disappear and causing an arrangement of the structure.

The variation of indirect and direct band gap reveals the presence of different types of coatings. These results using UV–vis spectroscopy are in good agreements with XRD results.

3.5 Corrosion Tests

3.5.1 Polarization curves

The behaviour of bare and multilayered ZnO/TiO_2 coated SS 304 substrates in chloride media are examined by means of polarization measurements in anodic and cathodic regions. The polarization curves obtained for SS304, bare and by different multilayered coatings are given in Figure 7. It can be seen that the corrosion potential E_{corr} was displaced to positive values for both $1ZnO/1TiO_2$ and $1TiO_2/1ZnO$ layers. Moreover, the current potential i_{corr} is found to decrease for coating layers which conduct to decrease the corrosion rate in this case and enhance the polarization resistance of SS 304 stainless steel. Meanwhile, when the bare substrate is coated by $2ZnO/2TiO_2$ and $2TiO_2/2ZnO$ layers, no protection is achieved; this can be confirmed by the displacement of E_{corr} to negative values as well as the increase in i_{corr} compared to the

bare metal. This can be explained as follow: SEM observations reveal that both of $2ZnO/2TiO_2$ and $2TiO_2/2ZnO$ layers contains cracks more than $1ZnO/1TiO_2$ and $1TiO_2/1ZnO$ layers, which allows Cl^- ions penetration through the coating layers and reach the metallic surface easily; hence the pitting corrosion starts. The development of this pitting leads thereafter to the deterioration of the protective layer ($2ZnO/2TiO_2$ and $2TiO_2/2ZnO$). Also, the penetration of pitting in the metal, which can be observed by the increase of the anodic current density (Figure 7**)** of $2ZnO/2TiO_2$ and $2TiO_2/2ZnO$ compared to the bare metal which forms a protective passive film, can protect it from pitting corrosion [33,34].

The electrochemical parameters calculated from polarization curves are presented in Table 3. By examining Table 3, it can be observed that $1ZnO/1TiO_2$ and $1TiO_2/1ZnO$ coatings are the most protective from corrosion, as can be confirmed by the decrease in corrosion rate values 0.0010 and 0.0052 mpy, respectively alongside with the increase in the polarization resistance *Rp* values 295 and 1030 kΩ. Also, it can be noticed that the best protective efficiency of 98% is achieved for $1TiO_2/1ZnO$ coating, where TiO_2 layer is in contact with the substrate SS 304 as well as with the corrosive medium; which can be explained by the higher resistance of TiO_2 layer compared to ZnO [35].

3.5.2 Electrochemical Impedance Spectroscopy Analysis

Protective properties of bare and coated SS 304 films in 0.5M NaCl solution are examined by electrochemical impedance spectroscopy (EIS) measurements; the obtained results are presented in Figure 8 in Nyquist plot. As can be clearly seen, the diameter of the loops obtained for coated SS304 stainless steel with $1ZnO/1TiO_2$ and $1TiO_2/1ZnO$ layers are significantly greater than bare metal and coated SS 304 with

$2ZnO/2TiO_2$ and $2TiO_2/2ZnO$ layers; i.e. the diameter of the loop is 185 times greater than that of bare substrate SS 304, which indicates an excellent protective properties.

The impedance spectra are fitted to the appropriate electrical equivalent circuit as shown in Figure 9 and the data are reported in Table 3, which is commonly used to simulate the corrosion behaviour of several coated metals systems [36-38], where Rs, Rc, Qc, Rt, Q_{dl} and W represent the resistance of the solution, the resistance of the coating, the constant phase element (CPE) of the coating, the charge transfer resistance and the CPE of double layer, and Warburg diffusion, respectively. CPE is used instead of pure capacitance due to the non-ideal character of the corresponding response [39].

The impedance spectra fitting of $2ZnO/2TiO_2$ coating presents a Warburg diffusion (Figure 9b), which can be attributed to a limited diffusion in coating/metal interface.

By examining Table 3, it can be noticed that the coating resistances Rc of different films are all above that of the bare substrate SS 304. However, Rc values of the two films $1ZnO/1TiO_2$ and $1TiO_2/1ZnO$ are the optimum values, which results in the increase in polarisation resistance Rp values especially for $1TiO_2/1ZnO$ film alongside with a decrease in Q_{dl} values. This confirms that both films exhibit the best corrosion performance.

Figure 10 shows the impedance spectra in Bode representation of bare metal and different multilayered ZnO/TiO_2coatings after 1 hour of immersion time in 0.5 M NaCl solution. The Bode impedance modulus (|Z|) (Figure 10a) at the low frequency region has been used to assess the barrier effectiveness and degradation behaviour of the coatings. This is because the corrosion reaction at the coating/metal interface takes place at this region [40].

It can be observed that the polarization resistance *Rp* increases for the two films $1ZnO/1TiO_2$ and $1TiO_2/1ZnO$**,** which can be observed from the increase in their modulus values. Figure10b illustrates the Bode phase angle plots of the EIS. It can be noticed that both $1ZnO/1TiO_2$ and $2TiO_2/2ZnO$ coatings exhibit one time constant, corresponding to the corrosion process occurring at the metal surface. In the case of $1TiO_2/1ZnO$ coating, two time constants can be observed; one can be attributed to TiO_2 protective film while the second is probably associated to the corrosion process occurring at the TiO_2/SS 304 interface [41]. Moreover, two time constants are observed for $2Zn/2TiO_2$ coating.

Lidija Curkovic et al. [14] attributed the appearance of time constant at low frequency (LF) to the films exhibiting a certain degree of porosity as corrosion process occurs on spots, where the electrolyte penetrates through the pores of the coating layer to the metal surface.

From the shape of the Bode plots, three different degradation stages are identified for all coatings. The obtained impedance values are given in Table 4. For the FDTS-free coating, it was observed that two time constants can be deduced after 1 h of immersion. The time constant at high frequencies (HF) is related to the responses of coatings in the solution (coating capacitance in parallel with its resistance), while the time constant at low frequencies (LF) is related to the corrosion process happening at the solution/metal interface in the pinholes of the coating (charge transfer resistance and double-layer capacitance) [20].

By examining Table 3, it can be noticed that the coating resistances Rc of different films are all above that of the bare substrate SS 304.

The obtained results (EIS plots and polarisation curves) are in good agreement with that EIS plots results and with Xu et al. [30] study. In the literature, Lidija Curkovic et al. [14] studied the electrochemical behaviour of TiO_2 thin films on SS 304 in 3.0% wt NaCl solution; they found that the polarization resistance Rp increase in the presence of TiO_2 film one and three layers**.** Suning Li and al. studied the effect of Ce-doped [31] and Cr-doped [32] nano-TiO_2 coatings (3 layers) on the corrosion protection of SS 316L, 3% NaCl in dark and under illumination. It was found that 1.2% Ce-doped nano-TiO_2 possesses excellent corrosion protection under illumination because of its higher e^-/H^+ pairs separation and photoelectric conversion efficiencies. This is due to: (i) 1.2% Ce-TiO_2 has anatase as dominating phase with smaller crystallite size 10.7 nm compared to pure TiO_2 having both anatase and rutile phases with 17.3 nm; (ii) TiO_2 contains some cracks with few pinhole-like defects while 1.2% Ce-TiO_2 has uniform surface and cracks-free. Ratchatee Techapiesancharoenkij et al. [19] studied the photocathodic protection of ZnO thick films (600-800 nm of thickness) deposited onto 304 SS while varying the substrate temperature (200 and 400 °C) in 3.0% wt NaCl solution. After polarization tests, they found that 200°C/ZnO thin film exhibited passivity (no peaks related to ZnO phase, dense nano-grains), while 400°C/ZnO showed no passivity and bad corrosion protection (wurtzite ZnO phase with preferred orientation along (002) plane, loosely compacted nano-granular needle-like shape) while the immersed 304 SS was completely corroded. Innocent O. Arukalam et al. [20] studied the anticorrosive behaviour of poly(dimethylsiloxane)-ZnO coatings (5 layers). It was found that the film with 0.10g (~0.19%) perfluorodecyltrichlorosilane (FDTS) exhibited the lowest rate of degradation, due to the remarkable improved crystallinity and hydrophobic character with maximum water contact angle value, resulting in

significant effect on the surface and barrier properties of the coatings. The $1TiO_2/1ZnO$ coated sample E_{corr} is -46 mV which is much higher than that of SS 304 with E_{corr} of -209 mV. Moreover, $1TiO_2/1ZnO$ coated sample gives a corrosion current density of 0.046 $\mu A.cm^{-2}$, which is lower than that SS 304 and coated samples of different thin coatings layers. In this study, the obtained results indicate that corrosion protection $1TiO_2/1ZnO$ coated SS 304 one layer by one layer exhibits the best corrosion protection for SS 304 in 0.5M NaCl with a protection efficiency of η=98%. This is achieved by the double protective layer (TiO_2/ZnO) forming a compact atomic arrangement and playing the role of an effective corrosion barrier against the dissolution of ions present in the corrosive medium.

4. Conclusion

Multilayered ZnO/TiO_2 coatings have been successfully deposited by sol-gel dip coating onto 304 SS stainless steel substrates. The effect of the layer nature (ZnO and TiO_2) and the order of the deposited layers on structure, surface topography, optical properties and corrosion performance in 0.5 M NaCl solution were investigated. XRD analysis confirms the formation of nanocrystalline ZnO and TiO_2 phases. SEM images indicate that the coatings are uniform, compact with few cracks. AFM analysis confirms the nanostructured aspect of the coatings. The obtained electrochemical measurements reveal that layer-by-layer coatings results in a significant improvement of the corrosion performance, reaching a very high protection efficiency of 98% for $1TiO_2/1ZnO$ coating. This has been associated with the synergetic combination of amorphous/nanocrystalline network-like structure and dense atomic arrangement

formed by the layered hexagonal/tetragonal crystal structures thus preventing the diffusion of corrosive ions through the surface.

Acknowledgments

The authors are thankful to Dr. Yazid Messaoudi from the University of Farhat Abbas Setif Algeria for his help in AFM analysis. Also, our thanks for Dr. Karima Abdelrahim from URASM El-Hadjar Annaba (Algeria), for her help in electrochemical measurements.

References

[1] P. Parthipan, P. Elumalai, J. Narenkumar, L.L. Machuca, K. Murugan, O.P. Karthikeyan, A. Rajasekar, Allium sativum (garlic extract) as a green corrosion inhibitor with biocidal properties for the control of MIC in carbon steel and stainless steel in oilfield environments, International Biodeterioration & Biodegradation 132 (2018) 66–73.

[2] P. Galliano, J.J.D. Damborenea, M.J. Pascual, A. Duran, Sol-gel coatings on 316L steel for clinical applications, Journal of Sol-Gel Science and Technology 13 (1998) 723–727.

[3] M. Mennig, C. Schelle, A. Duran, J.J. Damborenea, M. Guglielmi, G. Brustain, Investigation of glass-like sol-gel coatings for corrosion protection of stainless steel against liquid and gaseous attack, Journal of Sol-Gel Science and Technology 13 (1998) 717–722.

[4] M. Atik, M.A. Aegerter, Corrosion resistant sol-gel ZrO_2 coatings on stainless steel, Journal of Non-Crystalline Solids 147 & 148 (1992) 813-819.

[5] J. Masalski, J. Gluszek, J. Zabrzeski, K. Nitsch, P. Gluszek, Improvement in corrosion resistance of the 316l stainless steel by means of Al_2O_3 coatings deposited by the sol-gel method, Thin Solid Films 349 (1999) 186-190.

[6] J.R. Miranda, M.A.Sánchez, E.G. García, D.Y.M. Velazquez, and Á. de J.M. Ramírez, Mechanical Properties of SiO_2 Coatings for Corrosion Protection of 304 Stainless Steel, In book: Characterization of Metals and Alloys (2017) 109-116.

[7] T.T. Vu, L. del Rio, T. Valdes-Solis, G. Marban, Fabrication of wire mesh-supported ZnO photocatalysts protected against photocorrosion, Applied Catalysis B: Environmental 140–141 (2013) 189–198.

[8] A. Perez, A. Billard, C. Rebere, C. Berziou, S. Touzain, J. Creus, Influence of metallurgical states on the corrosion behaviour of Al–Zn PVD coatings in saline solution, Corrosion Science 74 (2013) 240–249.

[9] R. Hausbrand, B. Bolado-Escudero, A. Dhont, J. Wielant, Corrosion of flame assisted CVD silica-coated steel sheet, Corrosion Science 61 (2012) 28–34.

[10] A. Aouina, F. Bensouici, M. Bououdina, R. Tala-Ighil, M. Toubane, F. Kezzoula and K. Chebout, Effect of Er doping on the microstructural, optical, and photocatalytic activity of TiO_2 thin films, Materials Research Express 6 (2019) 016406.

[11] O.K. Echendu, S.Z. Werta, F.B. Dejene, V. Craciun, Electrochemical deposition and characterization of ZnO thin films for photovoltaic and photocatalysis applications, Journal of Alloys and Compounds 769 (2018) 201-209.

[12] M. Aparicio, A. Jitianu, G. Rodriguez, K. Al-Marzoki, M. Jitianu, J. Mosa, L.C. Klein, Thickness-properties synergy in organic – inorganic consolidated melting-gel coatings for protection of 304 stainless steel in NaCl solutions, Surface & Coatings Technology 315 (2017) 426 –435.

[13] S. Akhtar, A. Matin, A. M. Kumar, A. Ibrahim, T. Laoui, Enhancement of anticorrosion property of 304 stainless steel using silane coatings ,Applied Surface Science 440 (2018) 1286–1297.

[14] L. Curkovic, H.O.Curkovic, S. Salopek, M. Renjo , S. Segota, Enhancement of corrosion protection of AISI 304 stainless steel by nanostructured sol–gel TiO_2 films, Corrosion Science 77 (2013) 176–184.

[15] S.Q. Yu, Y.H. Ling, R.G. Wang, J. Zhang, F. Qin, Z.J. Zhang, Constructing superhydrophobic WO_3@TiO_2 nanoflake surface beyond amorphous alloy against electrochemical corrosion on iron steel, Applied Surface Science 436 (2018) 527–535.

[16] S.Y. Arman, H. Omidvar , S.H. Tabaian, M. Sajjadnejad, Sh. Fouladvanda, Sh. Afshar, Evaluation of nanostructured S-doped TiO_2 thin films and their photoelectrochemical application as photoanode for corrosion protection of 304 stainless steel, Surface & Coatings Technology 251 (2014) 162–169.

[17] D. Álvarez, A. Collazo, X.R. Nóvoa, C. Pérez, Assessment of ZnO nanoparticles as anticorrosive pigment in hybridsol–gel films, Progress in Organic Coatings 96 (2016) 3–12.

[18] A. Olad, R. Nosrati, Preparation and corrosion resistance of nanostructured PVC/ZnO–polyaniline hybrid coating, Progress in Organic Coatings 76 (2013) 113–118.

[19] R. Techapiesancharoenkij, W. Sripianem, K. Tongpul, C. Peamjharean, T. NaWichean, T. Meesak, P. Eiamchai, Investigation of the photocathodic protection of a transparent ZnO coating on an AISI type 304 stainless steel in a 3% NaCl solution, Surface & Coatings Technology 320 (2017) 97–102.

[20] I.O. Arukalam, M. Meng, H. Xiao, Y. Ma, E.E. Oguzie, Y. Li, Effect of perfluorodecyltrichlorosilane on the surface properties and anti-corrosion behavior of poly(dimethylsiloxane)-ZnO coatings, Applied Surface Science 433 (2018) 1113–1127.

[21 I.O. Arukalam, E.E. Oguzie , Y. Li, Fabrication of FDTS-modified PDMS-ZnO nanocomposite hydrophobic coating with anti-fouling capability for corrosion protection of Q235 steel, Journal of Colloid and Interface Science 484 (2016) 220‑228.

[22] M. Toubane, R. Tala-Ighil, F. Bensouici, M. Bououdina, M. Souier, S. Liu, W. Cai and A. Iratni, Sol concentration effect on ZnO nanofibers photocatalytic activity synthesized by sol–gel dip coating method, Materials Research Express 4 (2017) 035023.

[23] F. Bensouici, T. Souier , A. Iratni , A.A. Dakhel , R. Tala-Ighil , M. Bououdina, Effect of acid nature in the starting solution on surface and photocatalytic properties of TiO_2 thin films, Surface & Coatings Technology 251 (2014) 170–176.

[24] M. Toubane, R. Tala-Ighil, F. Bensouici, M. Bououdina, W. Cai, S. Liu, T. Souier, A. Iratni, Structural, optical and photocatalytic properties of ZnO nanorods: Effect of aging time and number of layers, Ceramics International 42 (2016) 9673–9685.

[25] F. Bensouici, M. Bououdina, A.A. Dakhel, R. Tala-Ighil, M. Tounane, A. Iratni, T. Souier, S. Liu, W. Cai, Optical, structural and photocatalysis properties of Cu-doped TiO_2thin films, Applied Surface Science 395 (2017) 110–116.

[26] F. Bensouici, M. Bououdina, A. Iratni, M. Toubane, and R.Tala-Ighil, Effect of thickness on photocatalytic activity of TiO_2 thin films, In book: Progress in Clean Energy, Volume 1, Chapter 56, 2015, pp. 763-776.

[27] F. Demichelis, G. Kanidakis, A. Tagliferro, E. Tresso, New approach to optical analysis of absorbing thin solid films, Applied Optics 9 (26) (1987) 1737-1740.

[28] A. Sharma, N. Mehta, A. Kumar, Dielectric relaxation in $Se_{80-x}Te_{20}Sn_x$ chalcogenide glasses, Journal Matter Science 46 (2011) 4509-4516.

[29]J. Tauc, F. Abeles, Optical Properties of Solids, North-Holland, Amsterdam, 1972.

[30] H. Xu, W. Liu, L. Cao, G. Su, R. Duan, Preparation of porous TiO_2/ZnO composite film and its photocathodic protection properties for 304 stainless steel, Applied Surface Science 301 (2014) 508-514.

[31] S. Li, Q. Wang, T. Chen, Z. Zhou, Y. Wang, J. Fu, Study on cerium-doped nano-TiO_2 coatings for corrosion protection of 316 L stainless steel, Nanoscale Research Letters 7(227) (2012) 1-9.

[32] S. Li, J. Fu, Improvement in corrosion protection properties of TiO_2 coatings by chromium doping, Corrosion Science 68 (2013) 101–110.

[33] L.F. Garfias-Mesias, J.M. Sykes, C.D.S. Tuck, The effect of phase compositions on the pitting corrosion of 25 Cr duplex stainless steel in chloride solutions, Corrosion Science 38(8) (1996) 1319-1330.

[34] P. Spathis, I. Poulios, the corrosion and photocorrosion of zinc and zinc oxide coatings, Corrosion Science 37 (5) (1995) 673-680.

[35] M.I Khan, K.A. Bhatti, R. Qindeel, L.G. Boussiakou, N. Alonizan, F. Aleem, Investigations of the structural, morphological and electrical properties of multilayer ZnO/TiO_2 thin films, deposited by sol-gel technique, Results in Physics 6 (2016) 156-160.

[36] M. Mrada, Y. Ben Amor, L. Dhouibia, M.F. Montemor, Corrosion prevention of AA2024-T3 aluminum alloy with a polyaniline/poly (γ-glycidoxypropyltrimethoxysilane) bi-layer coating: Comparative study with polyaniline mono-layer feature, Surface & Coatings Technology 337 (2018) 1–11.

[37] C. Liu, Q. Bi, A. Leyland, A. Matthews, An electrochemical impedance spectroscopy study of corrosion behaviour of PVD coated steels in 0.5 N NaCl aqueous solution: Part I. Establishment of equivalent circuits for EIS data modeling, Corrosion Science 45 (2003) 1243–1256.

[38] C. Liu, Q. Bi, A. Leyland, A. Matthews, An electrochemical impedance spectroscopy study of corrosion behaviour of PVD coated steels in 0.5 N NaCl aqueous

solution: Part II. EIS interpretation of corrosion behaviour, Corrosion Science 45 (2003) 1257–1273.

[39] H. Qian, D. Zhang, L. Deng, L. Huang, D. Xu, C. Du, X. Li, The role of surface morphology in the barrier properties of epoxy coatings in different corrosion environments, Progress in Organic Coatings 104 (2016) 199-209.

[40] W. Tian, F. Meng, L. Liu, Y. Li, F. Wang, Lifetime prediction for organic coating under alternating hydrostatic pressure by artificial neural network, Scientific Reports7 (2017) 40827.

[41] R.A. Antunes, M.C.L. de Oliveira, M.F. Pillis, Effect of the deposition temperature on the corrosion stability of TiO_2 films prepared by metal organic chemical vapour deposition, International Journal of Electrochemical Science 8 (2013) 1487–1500.

Table captions

Table 1. Crystallite size and microstrain of ZnO/TiO_2 multilayered thin films deposited onto glass substrates by sol-gel dip-coating followed by annealing at 450°C for 1 h as calculated by High Score program.

Table 2. AFM analysis data of ZnO/TiO_2 multilayered thin films deposited onto SS 304 stainless steel substrates.

Table 3. Potentiodynamic polarization parameters for bare and ZnO/TiO_2 multilayered thin films coated SS304 in 0.5 M NaCl.

Table 4. EIS fitting parameters for bare and ZnO/TiO_2 multilayered thin films coated SS 304 in 0.5 M NaCl.

Figure captions

Figure 1. XRD patterns of ZnO/TiO_2 mutilayered thin films deposited onto glass substrates by sol-gel dip-coating method followed by annealing at 450°C for 1 h.

Figure 2. Optical microscopy images of (a) SS 304 before and after coating with (b) ZnO/TiO_2, (c) TiO_2/ZnO, (d) $2ZnO/2TiO_2$; (e) $2TiO_2/2ZnO$.

Figure 3. SEM images of (a) SS 304 without and after coating with (b) ZnO/TiO_2, (c) TiO_2/ ZnO, (d) $2ZnO/2TiO_2$, (e) $2TiO_2/2ZnO$.

Figure 4. AFM images of images of (a) SS 304 without coating and after coating with (b) ZnO/TiO_2, (c) TiO_2/ ZnO, (d) $2ZnO/2TiO_2$, (e) $2TiO_2/2ZnO$.

Figure 5. UV-vis spectra of ZnO/TiO_2 multilayered thin films deposited onto glas substrates : (a) transmittance, (b) reflectance and (c) absorbance.

Figure 6. Plots of (a) $(\alpha hv)^2$ vs (hv) (b) and $(\alpha hv)^{0.5}$ vs (hv) of ZnO/TiO_2 multilayered thin films deposited onto glass substrates.

Figure 7. Tafel plots for ZnO/TiO_2 multilayered thin films deposited onto SS 304 substrates after 1h of immersion in 0.5 M NaCl solution.

Figure 8. Nyquist plots and the corresponding equivalent circuits for ZnO/TiO_2 multilayered thin films deposited onto SS 304 substrates after 1h of immersion in 0.5 M NaCl solution.

Figure 9. Equivalent electrical circuits used to model the impedance data: (a) bare SS 304, $1ZnO/1TiO_2$, $1TiO_2/ZnO$ and $2TiO_2/2ZnO$ films, (b) $2ZnO/2TiO_2$

Figure 10. Bode impedance plots for bare and of ZnO/TiO_2 multilayered thin films deposited onto SS 304 in 0.5 M NaCl (a) module plots and (b) phase angle plots.

Table 1

Coatings	**1ZnO/1TiO_2**	**1TiO_2/1ZnO**	**2ZnO /2TiO_2**	**2TiO_2/2ZnO**
Crystallite size (nm)	Amorphous	ZnO 14.99	TiO_2 6.94	ZnO 67.59 TiO_2 9.45
Microstrain (%)	Amorphous	ZnO 0.87	TiO_2 2.53	ZnO 0.19 TiO_2 1.90

Table 2

Sample	**SS 304 Substrate**	**1ZnO/1TiO_2**	**1TiO_2/1ZnO**	**2ZnO/2TiO_2**	**2TiO_2/2ZnO**
RMS (nm)	2.453	1.109	1.328	0.764	5.166
Average deviation (nm)	1.840	0.862	0.942	0.605	3.928
Skew (nm)	0.548	0.005	-1.240	0.348	0.730
Kurtosis (nm)	1.65	0.658	2.77	0.132	1.220

Table 3

Sample	E_{corr} (mV/SCE)	i_{corr} (μA/cm²)	beta c (mV/SCE)	beta c (mV/SCE)	Corrosion rate (mpy)	Rp (kΩ)	E (%)
SS 304	-209.303	2.291	306.6	235.8	0.0262	189	
1ZnO/1TiO_2	-123.653	0.090	183.5	429.4	0.0010	295	96.07
1TiO_2/1ZnO	-46.054	0.046	218.9	309.7	0.0052	1030	97.99
2ZnO/2TiO_2	-409.687	5.764	352,9	383.5	0.0660	*	#
2TiO_2/2ZnO	-420.029	5.853	446.5	213.5	0.0670	*	#

(*) For these two samples, the software is unable to determine the values because of bad corrosion protection.

(#) The values are insignificant because of bad corrosion protection.

Table 4

Sample	R_s ($\Omega.cm^2$)	R_c ($k.\Omega.cm^2$)	Q_c (μF)	n_1	R_p ($k\Omega.cm^2$)	Q_{dl} (μF)	n_2
SS 304	17.49	6. 164	5.305	0.94	67.53	56.11	0.75
1ZnO/1TiO_2	27,83	26. 963	4.87	0.86	810.00	10.99	0.81
1TiO_2/1ZnO	100	33. 590	1.046	0.98	1130.0	5.66	0.62
2ZnO/2TiO_2	19.55	7. 044	5.083	0.89	101.89	11.42	0.82
2TiO_2/2ZnO	50	7. 905	5.119	0.87	46.79	12.22	0.56

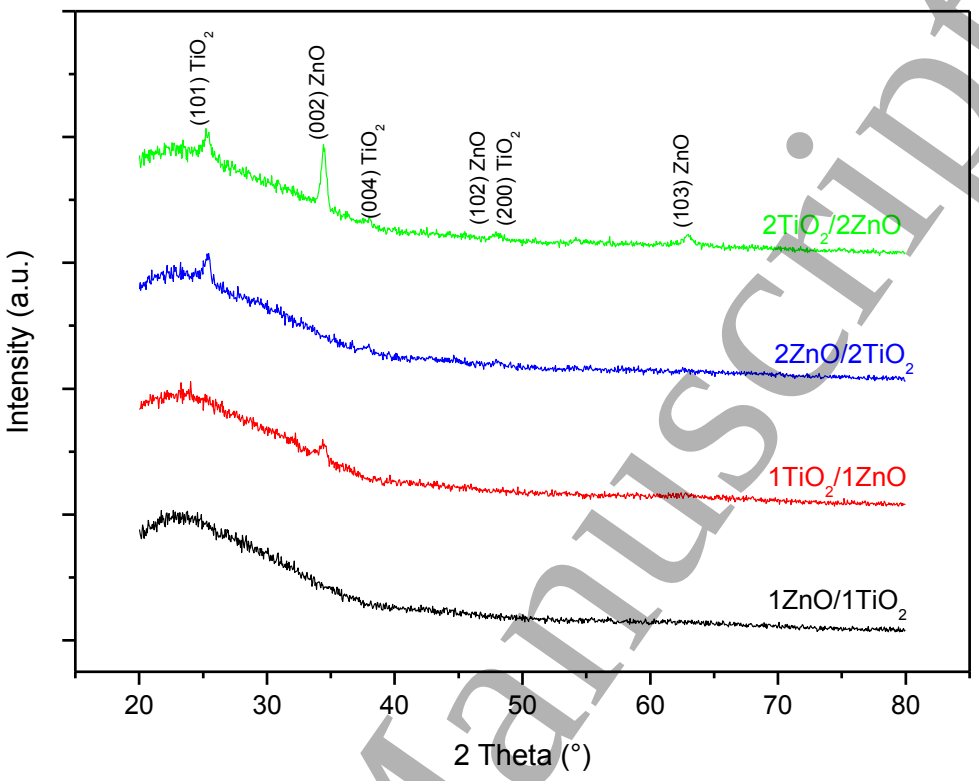

Figure 1

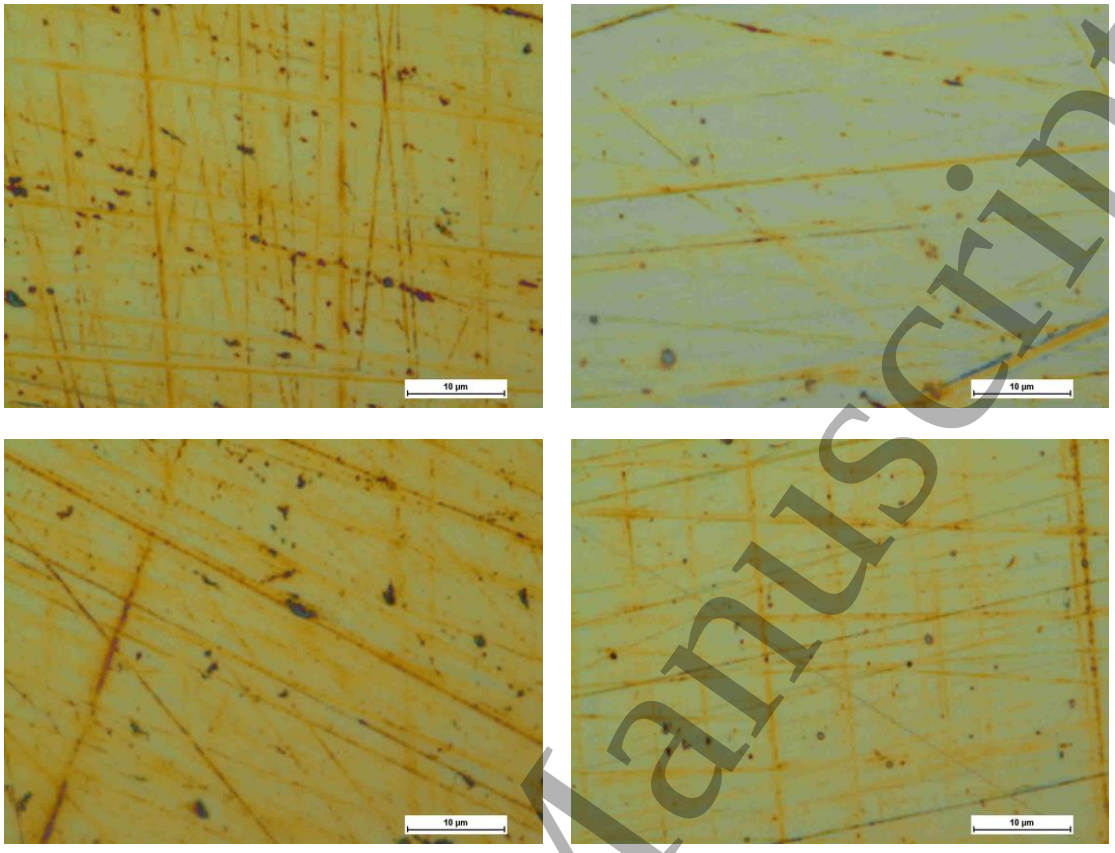

Figure 2

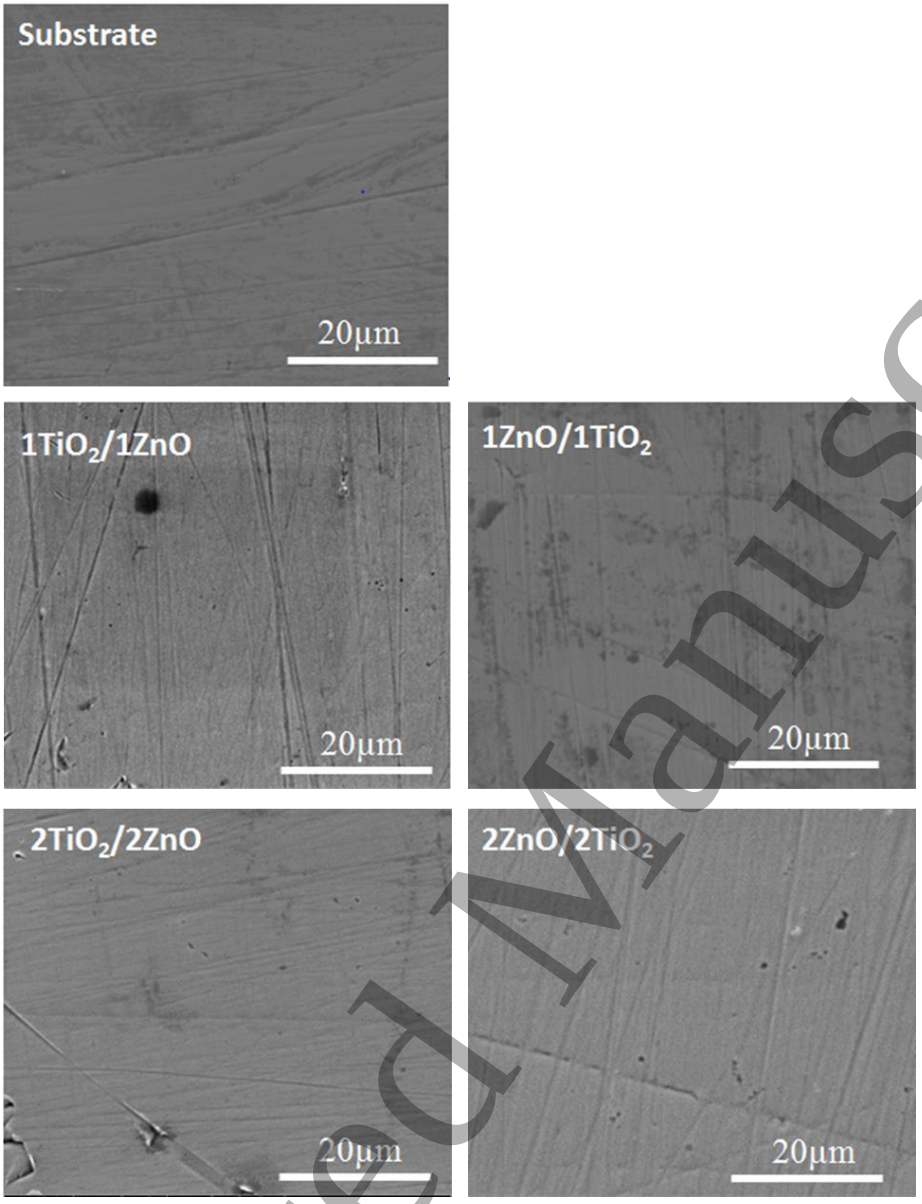

Figure 3

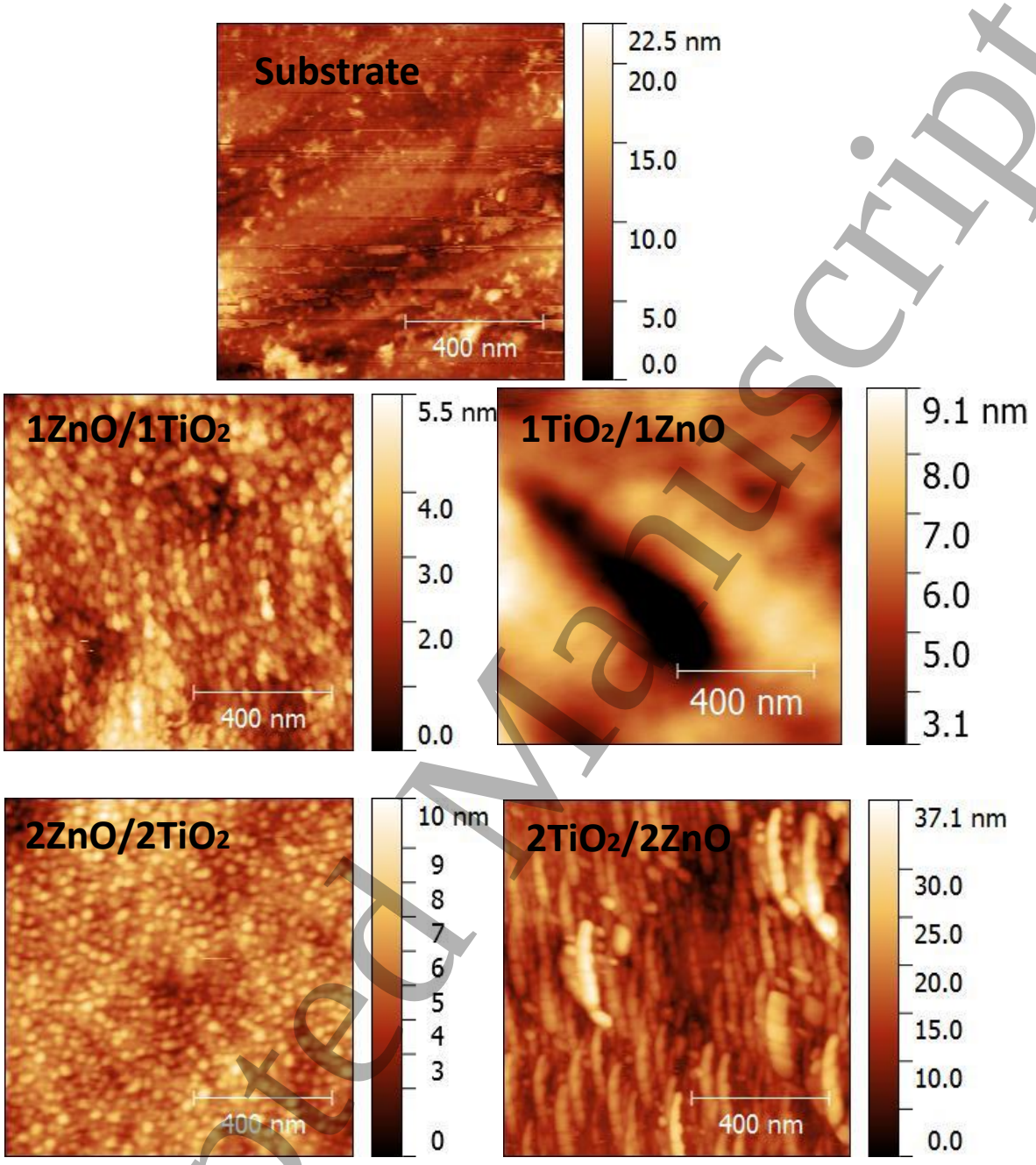

Figure 4

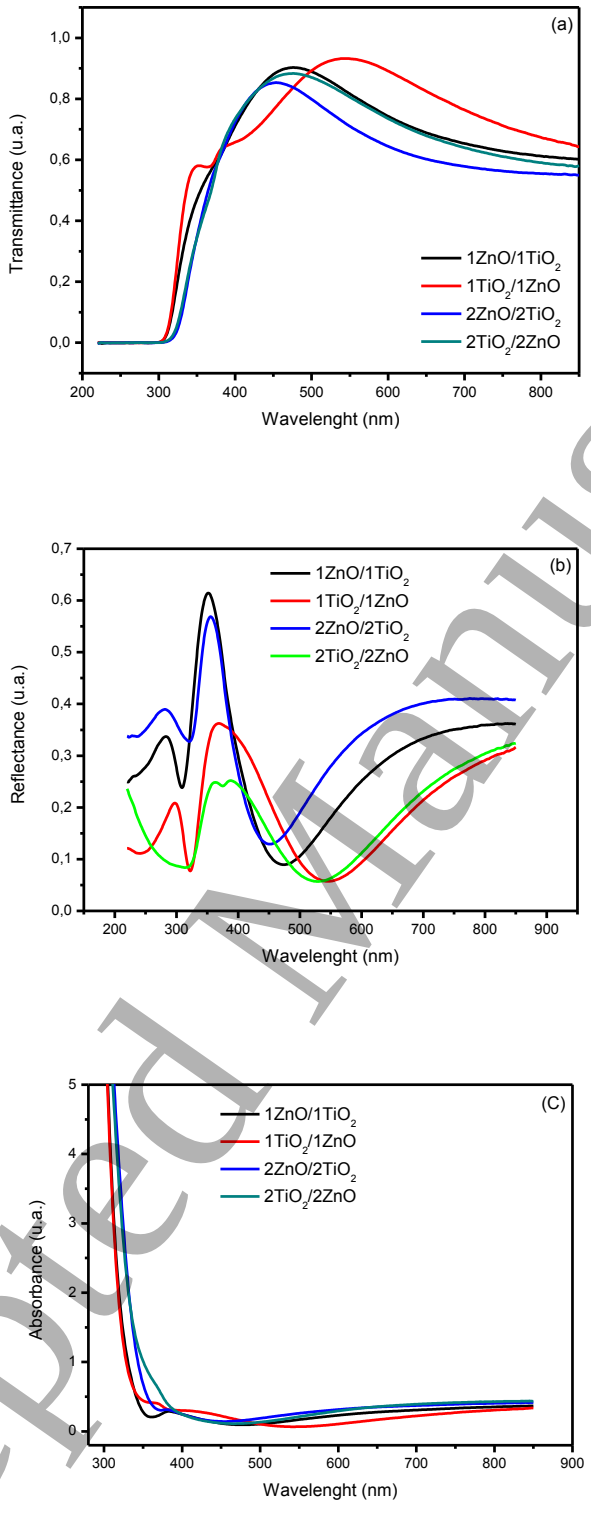

Figure 5

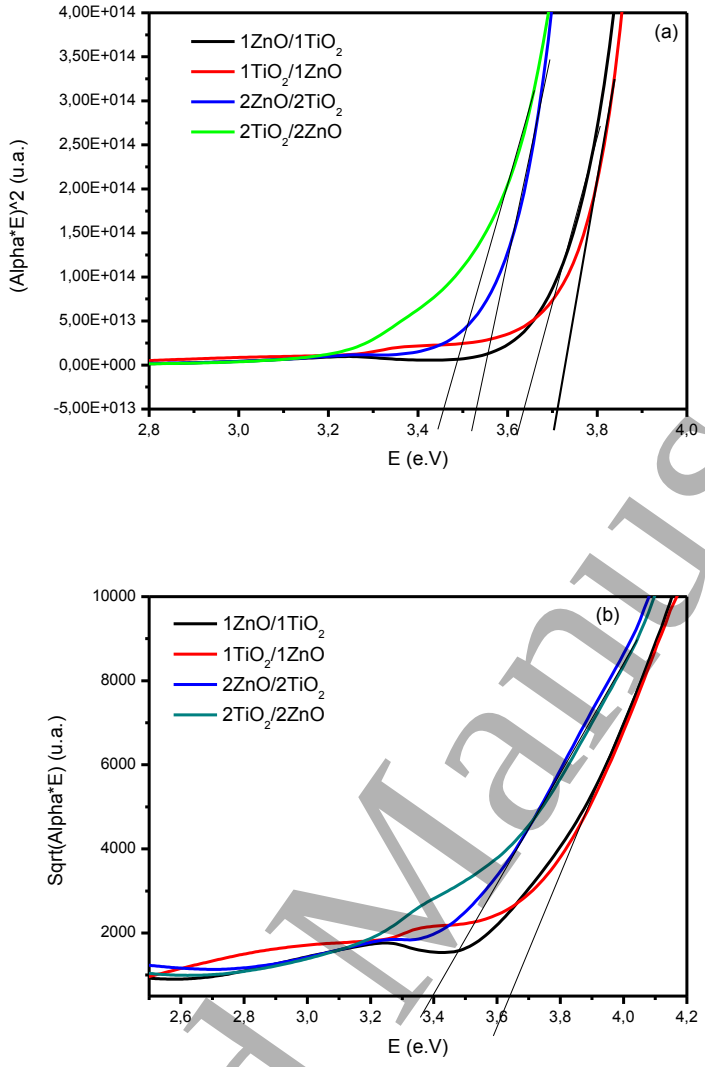

Figure 6

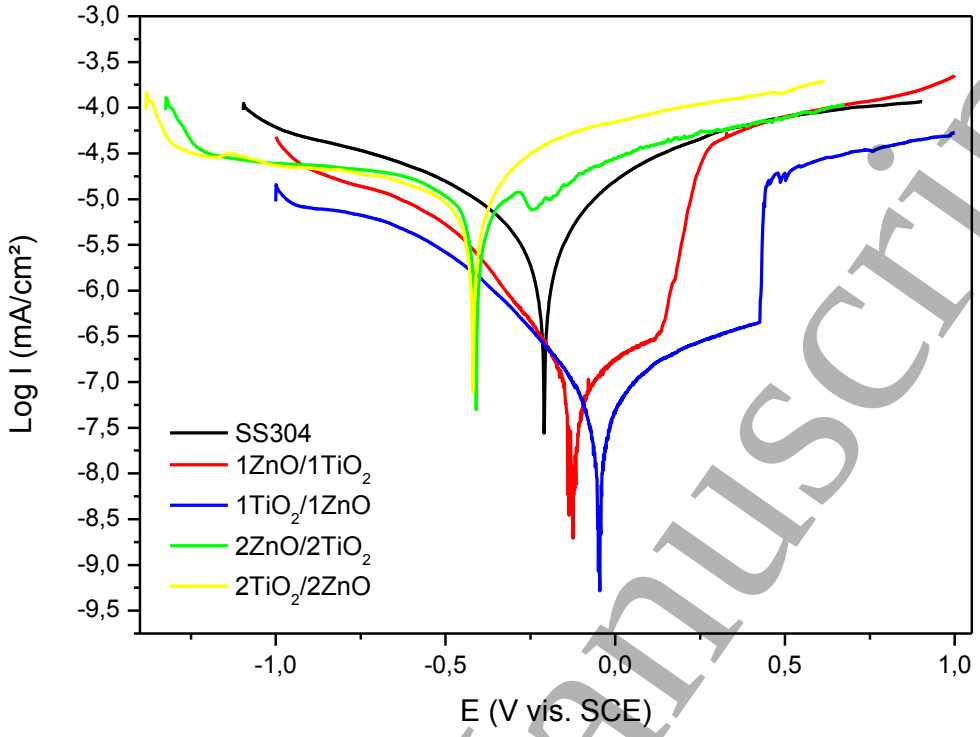

Figure 7

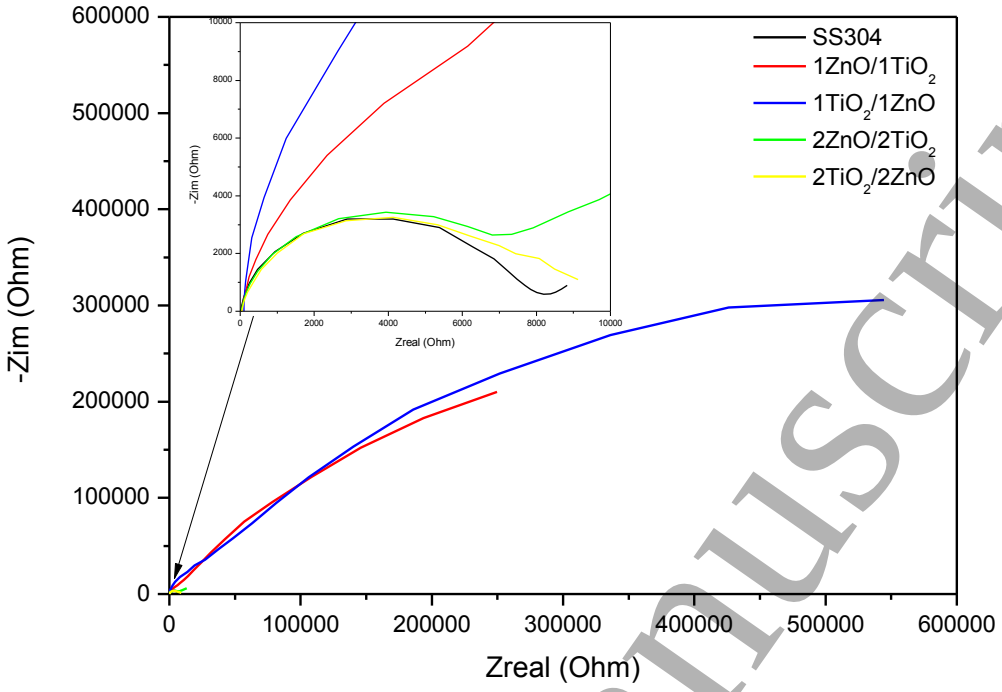

Figure 8

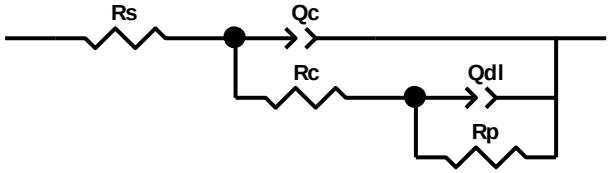

(a)

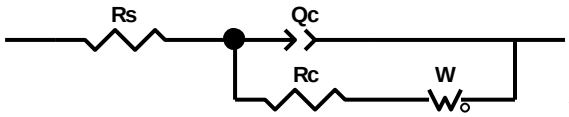

(b)

Figure 9

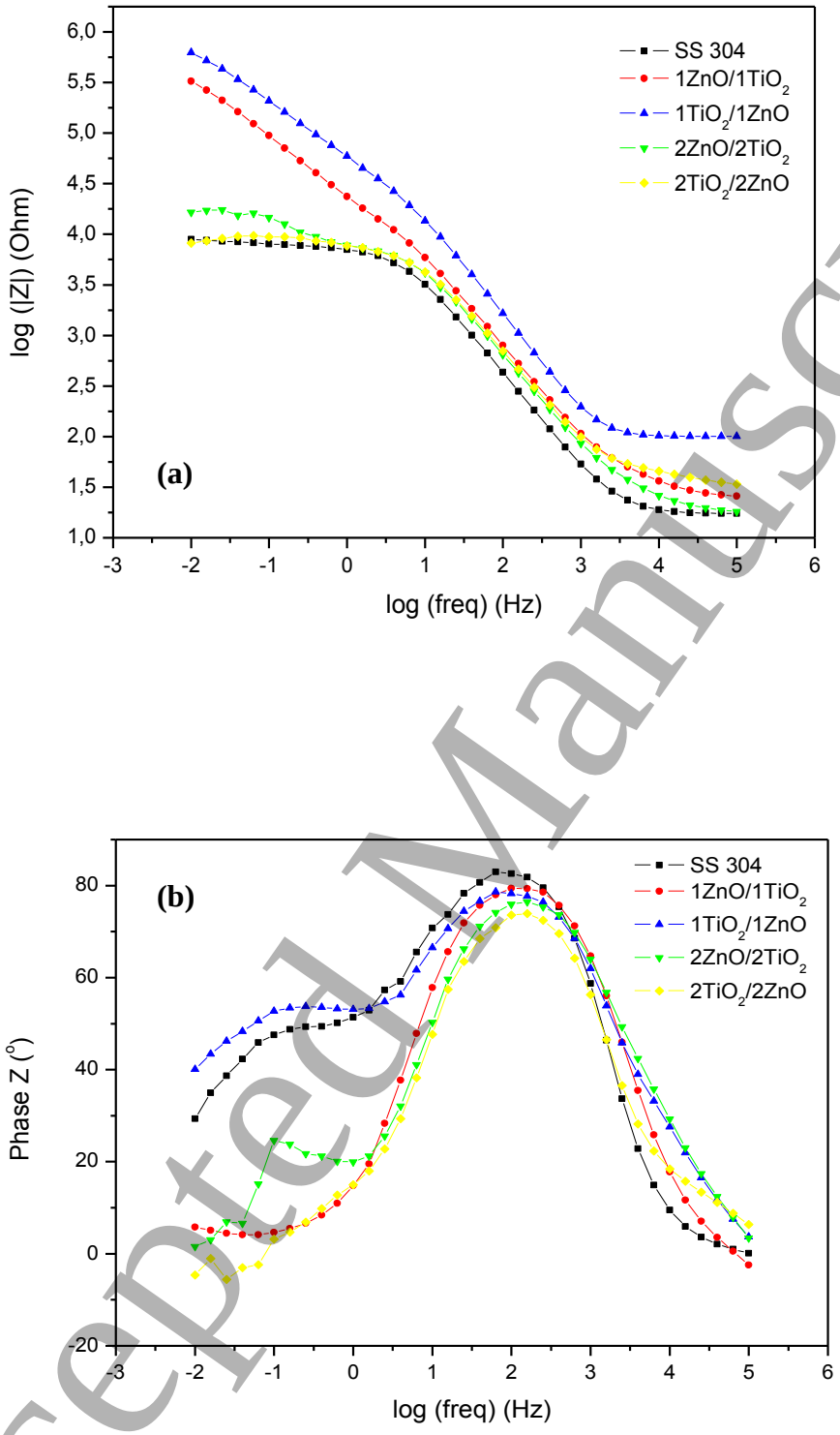

Figure 10